Phosphatidylinositol (4,5)-bisphosphate Impacts Ectosome Shedding from *C. elegans* Ciliated Sensory Neurons

Malek Elsayyid[1,2], Alexis E. Semmel[1,2], Nahin Siara Prova[1], Krisha D. Parekh[1], Jessica E. Tanis[1]

[1]Department of Biological Sciences, University of Delaware, Newark, Delaware, 19716

[2]These authors contributed equally

Correspondence:

Jessica E. Tanis
105 The Green
233 Wolf Hall
Newark, DE 19716
jtanis@udel.edu

Classification

Major category: Biological Sciences

Minor category: Cell Biology

Keywords

Cilia, PI(4,5)P2, PIP5K1, INPP5E, ectosome, extracellular vesicle, *C. elegans*

Significance

The membrane lipid phosphatidylinositol (4,5)-bisphosphate ($PI(4,5)P_2$) plays a critical role in many cellular processes including endocytosis, protein trafficking, cytoskeletal dynamics, ion channel activity, and cell polarity. Here we used a genetic approach to manipulate $PI(4,5)P_2$ levels in the primary cilium, a specialized sensory organelle that serves as a platform not only for organizing signal transduction, but also signal transmission via shedding of a class of extracellular vesicles, termed ectosomes. We discovered that high $PI(4,5)P_2$ differentially impacted shedding of two distinct EV subpopulations, decreasing biogenesis of ectosomes derived from the periciliary membrane compartment, but increasing budding from the cilium distal tip. This work defines a new role for $PI(4,5)P_2$ in the regulation of ectosome biogenesis and ciliary biology.

Abstract

Small secreted extracellular vesicles (EVs) mediate the intercellular transport of bioactive macromolecules during physiological processes and propagation of pathological conditions. The primary cilium, a sensory organelle protruding from most non-dividing cells, transmits signals by shedding EVs called ectosomes. Although the ciliary membrane is continuous with the plasma membrane, it exhibits unique phospholipid distribution, with levels of phosphatidylinositol 4,5-bisphosphate $PI(4,5)P_2$ high in the periciliary membrane compartment (PCMC), but low in the cilium proper and distal tip. The functional impact of $PI(4,5)P_2$ on ectosome biogenesis is not known. In *C. elegans* sensory neurons, different populations of ectosomes are shed from the PCMC and cilium distal tip. We used a genetic approach to increase $PI(4,5)P_2$ in the PCMC by overexpressing the type I phosphatidylinositol 4-phosphate 5-kinase (PIP5K1) PPK-1 or in the cilium proper through deletion of the phosphoinositide 5-phosphatase (INPP5E) *inpp-1*, then imaged released EVs that carried different fluorescently-tagged cargos. We discovered that high $PI(4,5)P_2$ differentially affected shedding of distinct ectosome populations from ciliary subcompartments, decreasing biogenesis of EVs from the PCMC, but increasing budding from the cilium distal tip. While manipulating $PI(4,5)P_2$ also impacted the trafficking, localization, and abundance of EV cargos in the cilium, localization of these proteins to distinct subsets of ectosome was unchanged, suggesting that $PI(4,5)P_2$ does not impact cargo sorting. Further, the $PI(4,5)P_2$-dependent increase in ectosome shedding from the distal tip did not alter cilium length. Thus, altering $PI(4,5)P_2$ serves as a mechanism to specifically regulate biogenesis of ectosomes shed in response to physiological stimulus.

Introduction

Non-motile primary cilia, sensory organelles enriched with receptors, ion channels, and effector molecules, provide a platform to detect and transduce external signals critical for development and cell homeostasis (1). More than thirty human diseases, termed ciliopathies, result from mutations in genes that encode proteins important for cilium structure or function (1). In addition to receiving signals, cilia can also transmit signals through the shedding of bioactive extracellular vesicles (EVs) (2–4). Cilia-derived EVs are utilized for multiple different purposes, including intercellular communication, transfer of signals between animals, regulation of ciliary signaling, and cell waste disposal (2–9). Thus, it is important to understand how EV biogenesis from this specialized organelle is regulated.

Contiguous with the plasma membrane, the periciliary membrane compartment (PCMC) at the ciliary base is separated from the cilium proper by the transition zone, which acts as a gate to confine proteins and lipids into the different compartments (1, 10, 11). Distinct phosphoinositides, generated by reversible phosphorylation and dephosphorylation of the inositol head groups, bind specific proteins to spatially regulate ciliary processes and signaling (12, 13). Phosphatidylinositol (4,5)-bisphosphate ($PI(4,5)P_2$) is concentrated in the plasma membrane and ciliary base, while phosphatidylinositol 4-phosphate (PI4P) is found at high levels in the cilium proper (13). This phosphoinositide compartmentalization is established by the action of type I phosphatidylinositol 4-phosphate 5-kinases (PIP5K1s), which generate $PI(4,5)P_2$ from PI(4)P (13–15), and the phosphoinositide 5-phosphatase INPP5E, which is enriched in the cilium proper and dephosphorylates $PI(4,5)P_2$ to produce PI4P (16–18). Loss of

INPP5E function is the underlying cause of two ciliopathies, Joubert syndrome and MORM syndrome, as well as ciliopathy phenotypes in mice and zebrafish (19, 20), demonstrating the significance of phosphoinositide compartmentalization in cilia biology.

Stimulation of quiescent cultured cells with serum results in removal of INPP5E from the primary cilium, leading to accumulation of PI(4,5)P_2 in the cilium proper. The increase in PI(4,5)P_2 causes actin polymerization and excision of the cilium distal tip, a process known as cilia decapitation, which results in loss of the primary cilium and cell cycle re-entry (21). This excision is distinct from the ectocytosis of small EVs, termed ectosomes, that bud directly from the periciliary membrane compartment (PCMC) and cilium distal tip (4, 6, 9, 22–24). Whether biogenesis of ciliary ectosomes is regulated by PI(4,5)P_2 as observed for ciliary decapitation remains unknown.

Shedding of bioactive EVs from sensory neuron cilia can be observed in living *C. elegans* (4, 22, 23, 25–28). Ectosomes that bud from the cilium distal tip play a role in animal-animal communication and are deposited on the vulva during mating (4, 5), while those shed from the PCMC of the ciliary base are taken up by surrounding glia or released into environment (23, 26). These two EV subpopulations, each with distinct signaling potentials, are differentially shed into the environment in response to the physiological stimulus of mating partners (22, 23). Ectocytosis of EVs derived from the cilium tip, but not the ciliary base, relies on redundant kinesin-2 motors required for intraflagellar transport. Together, this indicates that distinct regulatory mechanisms impact EV shedding from the cilium proper versus the ciliary base in a spatially-dependent manner.

Given the known impacts of PI(4,5)P_2 on protein localization, actin dynamics, endocytosis, exocytosis and membrane deformation (29), we reasoned that the ciliary

compartmentalization of $PI(4,5)P_2$ could have functional relevance for ectosome biogenesis. We found that the *C. elegans* type I phosphatidylinositol 4-phosphate 5-kinase PPK-1 localizes to and regulates $PI(4,5)P_2$ abundance in the ciliary base, while the *C. elegans* phosphoinositide 5-phosphatase INPP-1 localizes to and impacts $PI(4,5)P_2$ in the cilium proper of male-specific ray type B (RnB) EV-releasing neurons (EVNs). Using a genetic approach to manipulate $PI(4,5)P_2$ abundance in ciliary compartments of worms expressing fluorescently labeled EV cargos, we discovered that high $PI(4,5)P_2$ increases budding of EVs derived from the cilium tip, but inhibits biogenesis of an EV subpopulation shed from the PCMC. This altered EV biogenesis is not accompanied by a change in cilium length, suggesting that increasing $PI(4,5)P_2$ in the cilium proper can serve as a mechanism to enhance EV ectocytosis from the distal tip without inducing ciliary decapitation.

Results

Ciliary $PI(4,5)P_2$ is regulated by PPK-1 and INPP-1 activity in EV-releasing neurons

Like in other organisms, $PI(4,5)P_2$ has been shown to be depleted in the cilium proper of certain *C. elegans* ciliated sensory neurons, though the abundance of this phosphoinositide in the sensory cilia of the EV-releasing neurons (EVNs) had not been explored. The cilia of the EVNs, which include the inner labial type 2 (IL2), male-specific ray type B (RnB), hook B (HOB), and cephalic male (CEM) neurons, have microtubules with specialized structure and post-translational modifications as well as distinct motor proteins that enable abundant EV shedding from the cilium distal tip (Fig. 1A) (28, 30, 31). To determine if the EVN cilia exhibit phosphoinositide compartmentalization as

observed for other neurons, we used the *klp-6* promoter (32) to drive expression of a PI(4,5)P_2 reporter consisting of the PH domain of phospholipase C delta 1 fused to mNeonGreen (mNG::PLCδ1-PH) in IL2 and male ciliated sensory neurons (11, 33). We co-expressed this integrated mNG::PLCδ1-PH transgene with mScarlet-tagged MKS-2 (MKS-2::mSc), a protein in the Meckel syndrome (MKS) complex that localizes to the transition zone (34). We found mNG::PLCδ1-PH localized to the distal dendrite and PCMC, which is similar to the ciliary pocket in mammals (35), but was excluded from the cilium proper of the RnB neurons (Fig. 1B). This demonstrates that the EVN cilia use the same phosphoinositide code as other sensory cilia.

In *C. elegans* the sole PIP5K1, PPK-1, generates PI(4,5)P_2 both *in vitro* and *in vivo* and is strongly expressed in the nervous system (14). GFP-tagged PPK-1 was previously shown to have a localization pattern similar to that of GFP::PLCδ1-PH in the AWB sensory neurons, though this reporter was not expressed at endogenous levels or imaged with a transition zone marker (33). To define where PPK-1 is localized in the EVNs, we inserted an N-terminal mNG tag on *ppk-1* (mNG::PPK-1) at the endogenous locus and isolated viable animals. This indicates that mNG::PPK-1 is a functional fusion protein, as loss of *ppk-1* results in lethality due to its essential role in embryogenesis (14). Coexpression of mNG::PPK-1 and MKS-2::mSc showed that PPK-1 was present in the dendrite and PCMC, with significantly lower abundance in the cilium proper (Fig. 1C; Sup. Fig. S1A). We next examined the localization pattern of INPP-1, the *C. elegans* ortholog of INPP5E, which hydrolyses the 5-phosphate from PI(4,5)P_2. Previously, overexpressed INPP-1::GFP was shown to be present at similar level in the AWB neuron dendrite, PCMC, and cilium (33). However, images of endogenous INPP-1 tagged with mNG at the C-terminus

(INPP-1::mNG), coexpressed with MKS-2::mSc, showed abundant INPP-1 in the cilium proper and transition zone, with a significant dip in abundance in the PCMC (Fig. 1D; Sup. Fig. S1B). Together, our data show ciliary compartmentalization of enzymes that regulate $PI(4,5)P_2$ levels in the EVNs.

We next sought to determine how altering levels of PPK-1 and INPP-1 impacted $PI(4,5)P_2$ abundance in the PCMC and cilium. Since *ppk-1* deletion mutants arrest as larvae, we instead used a transgene to overexpress PPK-1 in neurons (14) and found that this caused a significant increase in $PI(4,5)P_2$ in the dendrite and PCMC, with minimal impact on $PI(4,5)P_2$ in the cilium proper (Fig. 1E-G). Previously, loss of INPPE in mammalian cells and loss of *inpp-1* in *C. elegans* AWB neurons has been shown to cause significant accumulation of $PI(4,5)P_2$ in primary cilia. Consistent with this, we observed mNG::PLCδ1-PH in the cilium proper of *inpp-1* mutant RnB neurons, but not wild-type animals (Fig. 1E-G). This indicates that PPK-1 and INPP-1 work together to partition $PI(4,5)P_2$ in the EVNs (Fig. 1H).

An increase in PCMC $PI(4,5)P_2$ reduces ectosome shedding from this compartment

Having established that overexpression of PPK-1 causes an increase in $PI(4,5)P_2$ in the PCMC of the ciliary base (Fig. 2A), we sought to determine how this impacts EV shedding. The CLHM-1 and PKD-2 ion channels are found in discrete EV subpopulations, with CLHM-1 packaged into EVs shed from the PCMC of the ciliary base and PKD-2 loaded into EVs predominantly shed from the cilium distal tip (22, 23). We crossed the PPK-1 overexpression transgene with tdTomato-tagged CLHM-1 (CLHM-1::tdT) and GFP-tagged PKD-2 (PKD-2::GFP) single copy transgenes as well as *him-5(e1490)*, which

causes increased frequency of X chromosome nondisjunction, leading to male offspring for analysis (36). Using total internal reflection fluorescence (TIRF) microscopy, we imaged EVs released into the environment from male tail EVNs (Fig. 2B,C; Sup. Fig. 3) and discovered that overexpression of PPK-1 caused a decrease in shedding of the CLHM-1 EV subpopulation, but had no impact on the PKD-2 EV abundance (Fig. 2D,E). We next examined the colocalization of the ion channel cargoes in EVs and found that the probability of PKD-2::GFP being found in a CLHM-1::tdT EV was unchanged by PPK-1 overexpression (Fig. 2F). This suggests that while the overall shedding of these PCMC-derived EVs is reduced, the sorting of cargos into the EVs is not disrupted.

PI(4,5)P_2 abundance impacts trafficking of ciliary proteins as well as endocytosis. To determine if an increase in PCMC PI(4,5)P_2 had an effect on EV cargo localization, we crossed the PPK-1 overexpression transgene together with CLHM-1::tdT and MKS-2::mNG and quantitated CLHM-1::tdT fluorescence intensity and volume in the different ciliary compartments (Sup. Fig. S2). While CLHM-1 was present in the PCMC of all control RnB neurons analyzed, 34% of the RnBs in the PPK-1 overexpressor lacked any detectable CLHM-1 in the PCMC (Fig. 2G,H). Overall, PPK-1 overexpression reduced CLHM-1 in the ciliary base, but had very minimal impact on CLHM-1 in the cilium proper, indicating that trafficking of this protein was not affected (Fig. 2I,J). This suggests that reduced or absent CLHM-1 in the PCMC is likely due to an increase in endocytosis, as internalization of channels via clathrin-mediated endocytosis requires PI(4,5)P_2. While reduced CLHM-1 in the ciliary base may explain the decrease in shedding of EVs with this cargo (Fig. 2E), we note that a reduction in CLHM-1 abundance in this compartment does not always correlate with a decrease in the number of shed EVs (23). Analysis of

ciliary PKD-2::GFP showed that PPK-1 overexpression disrupted relative abundance of PKD-2 in the different ciliary compartments and resulted in a higher level in the transition zone, indicating an impact on trafficking (Fig. 2K-M). In conclusion, these data highlight multiple impacts of $PI(4,5)P_2$, reducing EV cargo abundance and shedding from the PCMC.

Elevated $PI(4,5)P_2$ in the cilium proper increases EV release from the ciliary tip

Unlike INPP5E mutant mice, which die soon after birth, *inpp-1* mutant *C. elegans* appear essentially normal, but do accumulate $PI(4,5)P_2$ in the cilium proper (Fig. 1E-G; Fig. 3A). We found that loss of *inpp-1* significantly increased the shedding of the cilium tip-derived PKD-2::GFP ectosomes from the male tail EVNs (Fig. 3B-D; Sup. Fig. 4A). However, the average number of CLHM-1::tdT EVs as well as the probability of PKD-2::GFP being present in a CLHM-1::tdT EV was unchanged between wild-type and the *inpp-1* mutant (Fig. 3E,F). Given the impact of INPP-1 on PKD-2::GFP EV shedding, we next examined ciliary PKD-2::GFP distribution in RnB neuron cilia and found that PKD-2::GFP was absent from the cilium proper and tip in 24% of the *inpp-1* mutant cilia examined, a significantly higher percentage than observed for wild type (Fig. 3G,H). While the average intensity and volume of ciliary PKD-2::GFP was unchanged by loss of *inpp-1* (Fig. 3I,J), analysis of only the cilia that contained PKD-2::GFP showed a significant increase in PKD-2::GFP fluorescence intensity in the *inpp-1* mutant (Fig. 3H, Sup. Fig. S4B). Together, these results suggest that $PI(4,5)P_2$ accumulation in the cilium proper increases the shedding of PKD-2-containing EVs, which may impact the abundance of this protein in the cilium proper.

An increase in ciliary PI(4,5)P_2 does not impact EVN cilium length

Altering PI(4,5)P_2 in the cilium proper has been shown to act as a mechanism to regulate cilium length by impacting membrane stability and turnover (18, 20, 37) and highly elevated PI(4,5)P_2 in the cilium proper results in excision of the cilium distal tip, leading to loss of the cilium (21). To determine if the PI(4,5)P_2-dependent changes in EV biogenesis impact the length of the cilium, we used KLP-6::GFP to completely fill out the RnB neurons and labeled the TZ with MKS-2::mSc, then measured cilium length post-TZ in PPK-1 overexpressor, *inpp-1* mutant, and control animals. Altering PI(4,5)P_2 abundance did not significantly alter the length of the cilium proper for three different classes of RnB neurons analyzed, although higher variability was observed in the *inpp-1* deletion mutant (Fig. 4A,B; Sup. Fig. 4C,D). These data show that an increase in PI(4,5)P_2 in the cilium proper does not cause ciliary decapitation or shortening of the EVN cilia. This suggests that the lack of PKD-2 in 24% of the *inpp-1* mutant RnB cilia (Fig. 3G) may instead be due to altered trafficking or the release of all cilium PKD-2::GFP into ectosomes via increased ciliary shedding (Fig. 3D, Sup. Fig. 4A,B).

Discussion

The phosphoinositide PI(4,5)P_2 plays critical roles in protein localization, endocytosis, and membrane deformation (29). Here, using fluorescently-tagged cargoes to visualize EVs, we show for the first time that PI(4,5)P_2 also impacts shedding of signaling ectosomes. High PI(4,5)P_2 levels differentially impacted two distinct EV subpopulations, decreasing

biogenesis of CLHM-1 containing ectosomes derived from the PCMC, but increasing budding of PKD-2 EVs from the cilium distal tip (Fig. 4C). Reduced EV shedding from the PCMC was correlated with lower abundance of the EV cargo in the ciliary base, suggesting that endocytosis and ectosome budding from the PCMC are coupled to regulate ciliary protein content (Fig. 4C). In contrast, an increase in ciliary $PI(4,5)P_2$ did not cause mislocalization of cargoes within the cilium or the length of the cilium, indicating that $PI(4,5)P_2$-dependent modulation of ectosome shedding from this site has potential to regulate EV-mediated signaling. Together, this shows a new role for the phosphoinositide $PI(4,5)P_2$ in ciliary ectosome biogenesis.

Maintenance of low $PI(4,5)P_2$ in the cilium enables the $PI(4,5)P_2$-binding Tubby (TUB) and Tubby-like (TULP) proteins, which link ciliary membrane proteins to the intraflagellar transport (IFT) system, to mediate precise trafficking of ciliary proteins including ion channels and G-protein coupled receptors (16, 17, 33, 38, 39). Nevertheless, how compartmentalization of phosphoinositides in different ciliary compartments is established and maintained is not completely understood. Here we show that localization of PPK-1 and INPP-1 to the ciliary base and cilium proper, respectively, regulates $PI(4,5)P_2$ in EVN cilia subcompartments. Loss of the TZ protein MKS-5 results in abnormal $PI(4,5)P_2$ accumulation in the cilium proper (11), though whether this is due to mislocalization of these $PI(4,5)P_2$ regulatory enzymes, or because an intact TZ acts as a lipid diffusion barrier (10) is unknown. Interestingly, TZ mutants also have defects in EV shedding (27, 41), which could result from loss of $PI(4,5)P_2$ compartmentalization. Future work assessing both the abundance and localization of $PI(4,5)P_2$, INPP-1, and PPK-1 in TZ mutants would shed light on the mechanism by which specific TZ proteins contribute

to the ciliary compartmentalization of PI(4,5)P_2, which impacts both protein trafficking and ectosome release.

PPK-1 overexpression did not impact CLHM-1 localization to the cilium proper, likely because transport of this protein is not dependent on kinesin-2-mediated IFT for trafficking into the cilium (23). However, overexpression of PPK-1 did cause a significant shift of PKD-2 into the transition zone, indicative of altered IFT-dependent trafficking. Further, analysis of only the neurons with PKD-2::GFP present in the cilium proper showed that loss of *inpp-1* increased ciliary abundance of this protein. This is consistent with observations seen in INPP5E-depleted neural stem cells and mouse embryonic fibroblasts, in which PI(4,5)P_2 buildup altered ciliary trafficking and increased abundance of the G protein-coupled receptor Gpr161 in the cilium proper (16, 17). This leads us to suggest that increasing PI(4,5)P_2 in the cilium proper can be used as a mechanism to increase in EV biogenesis from the cilium distal tip, reducing ciliary membrane protein content when trafficking of ciliary membrane proteins is disrupted.

EV shedding can affect protein composition of the cilium and remove activated receptors to control signaling in the releasing cell (6), while uptake of EVs can impact signaling in surrounding cells (24) and play a role in inter-organism communication (4, 5). How might ciliary abundance and compartmentalization of PI(4,5)P_2 be controlled in living animals to regulate ectosome release? External stimuli can dynamically regulate protein content in both the cilium proper and EVs (6, 22, 23, 33). Interestingly, compromised sensory signaling in the ciliated sensory AWB neurons increases trafficking of PPK-1 into the cilium proper, and thus, PI(4,5)P_2 (33). This raises the possibility that sensing of mate availability, which impacts EV release (22, 23), or other mating cues (40) by the EVNs,

could alter the localization, abundance or activity of the proteins that regulate PI(4,5)P_2 levels to regulate both ciliary localization of EV cargoes and ectosome shedding.

INPP5E mutations in humans cause cilium instability and signaling defects, resulting in ciliopathy syndromes (19, 20). Loss of *Inpp5e* or rapid synthesis of PI(4,5)P_2 in the cilium proper has previously been shown to reduce cilia length through a process known as ciliary decapitation (20, 21, 37). We found that the increase in cilium PI(4,5)P_2 and tip-derived EV shedding in the *inpp-1* mutant did not change RnB neuron cilium length, suggesting that the increase in PI(4,5)P_2 and EV transmission does not impact the morphology of these cilia. It remains possible that there is a redundant phosphatase that prevents PI(4,5)P_2 from reaching a level that would induce ciliary decapitation. Multiple other phosphoinositide 5-phosphatases, including OCRL and INPP5B that can dephosphorylate PI(4,5)P_2, localize to primary cilia in other organisms (20, 41, 42). Knockdown of OCRL1 in cultured cells and zebrafish causes ciliary defects (43, 44), while loss of INPP5B alters ciliary length and number (45). We tagged *C. elegans* OCRL-1 and the INPP5B ortholog CIL-1 with mNeonGreen at the endogenous loci, but did not observe localization to the cilium proper in the EVNs (data not shown). While we cannot rule out the presence of additional phosphoinositide 5-phosphatases, we suggest that since the EVNs are terminally differentiated cells, an increase in PI(4,5)P_2 in the primary cilium may be used to regulate ectosome release rather than induce ciliary decapitation.

Limitations of the Study

EV shedding can change the protein composition within the cilium to regulate signal transduction (6) and transmit a signal to surrounding cells (26) and nearby animals (5). Since PI(4,5)P_2 regulates ciliary localization and abundance of EV cargoes via protein trafficking and endocytosis (6, 16, 17, 33) as well as ectosome shedding, it is not possible to determine if any changes in behavior that might result from altered PI(4,5)P_2 levels or compartmentalization is due to the signaling potential of released EVs or altered abundance of EV cargoes in the cilium proper. These impacts are not mutually exclusive, supporting the idea that PI(4,5)P_2 is a global regulator of cilia biology, with this work showing that it can impact ectosome biogenesis.

Figure legends

Figure 1. PPK-1 and INPP-1 regulate PI(4,5)P_2 abundance and localization in sensory cilia. (A) Schematic of EV shedding from the cilium distal tip and PCMC of the cilium base into the environment from male tail *C. elegans* RnB sensory neurons. (B) In control (*him-5* mutant) males, the PI(4,5)P_2 sensor mNG::PLCδ1-PH (top) is absent from the RnB cilium proper; MKS-2::mSc (middle) shows the transition zone (TZ). Right, normalized fluorescence intensity of mNG::PLCδ1-PH along n = 28 RnB cilia. (C) mNG::PPK-1 (top) and MKS-2::mSc (middle) in a RnB neuron. Normalized mNG::PPK-1 fluorescence intensity (right) shows abundant PPK-1 in the dendrite and ciliary base with significantly less in the cilium proper; n = 29 cilia. (D) INPP-1::mNG (top) localizes to the cilium proper, TZ (MKS-2::mSc; middle), and distal dendrite. INPP-1::mNG fluorescence (right; normalized) is reduced in the ciliary base; n = 23 cilia. (E) mNG::PLCδ1-PH and

MKS-2::mSc in wild-type, PPK-1 overexpression (two representative images), and *inpp-1(gk3262)* loss of function mutant (Δ*inpp-1*) animals; identical settings used for all images. (F) Percent of neurons with mNG::PLCδ1-PH in the cilium proper. PI(4,5)P_2 was present in the cilium proper of all *inpp-1* mutant RnBs analyzed; n = 23 cilia; **** p < 0.0001. (G) mNG::PLCδ1-PH fluorescence intensity in control (grey), PPK-1 overexpressor (purple), and *inpp-1* mutant (orange) animals; n ≥ 22 cilia. PPK-1 overexpression greatly increases the abundance of PI(4,5)P_2 in the ciliary base; loss of *inpp-1* results in high PI(4,5)P_2 in the cilium proper (H) Diagram showing INPP-1 and PPK-1 localization as well as how these enzymes affect ciliary PI(4,5)P_2 levels in wild type animals. In all images (B-E), the cilium distal tip is oriented to the left; scale, 2 μm. Data are presented as mean +/- SEM.

Figure 2. PPK-1 regulates CLHM-1 EV shedding and ciliary localization (A) Schematic depicting high ciliary base PI(4,5)P_2 in PPK-1 Oex animals. (B-C) Representative images of CLHM-1::tdT (*henSi3*) and PKD-2::GFP (*henSi20*) EVs released from (B) control and (C) PPK-1 Oex animals. EVs are marked with spots (Imaris software) for visualization; original images are in Sup. Fig. S3; scale, 10 μm. (D) PKD-2::GFP EV release is not affected by PPK-1 Oex; n ≥ 26. (E) Release of CLHM-1::tdT EVs decreases in PPK-1 Oex animals; n ≥ 26, * p < 0.05. (F) Probability of PKD-2::GFP presence in CLHM-1::tdT EVs is unchanged by PPK-1 Oex; n ≥ 26. (G) PPK-1 Oex reduces percent of RnBs with CLHM-1::tdT in the PCMC; n ≥ 41. (H) CLHM-1::tdT (top) and MKS-2::mNG (middle) localization in cilia of control and PPK-1 Oex animals. Cilium proper oriented to the left, two representative images shown for the PPK-1 Oex (a, b) to show the different phenotypes observed; scale, 2 μm. (I) Mean fluorescence

intensity and (J) volume of CLHM-1::tdT in the PCMC and cilium proper in control and PPK-1 Oex animals; n ≥ 41. (K) PKD-2::GFP (top) and MKS-2::mSc in control and PPK-1 Oex animals. (L) Quantification of PKD-2::GFP fluorescence intensity shows altered localization in the PPK-1 Oex (purple) compared to control (grey); n ≥ 14. (M) Percent of MKS-2::mSc TZ volume that overlapped with PKD-2::GFP; n ≥ 23. In this figure, data are represented as mean +/- SEM; Mann-Whitney test, * $p < 0.05$, **** $p<0.0001$.

Figure 3. INPP-1 regulates PKD-2 EV release and ciliary localization. (A) Schematic showing high $PI(4,5)P_2$ in both the PCMC and cilium proper in the *inpp-1* mutant. (B-C) Representative images of CLHM-1::tdT and PKD-2::GFP EVs shed from (B) control and (C) *inpp-1* mutant male tails; scale, 10 μm. EVs marked with spots (Imaris software) for visualization; see also Sup. Fig. 3. (D) Loss of *inpp-1* causes an increase in the number of PKD-2::GFP EVs, but does not impact (E) CLHM-1::tdT EV shedding or (F) colocalization of the two cargos in EVs; n ≥ 25. (G) Significantly fewer *inpp-1* mutants exhibited PKD-2::GFP in the cilium proper compared to the control; n ≥ 44. (H) PKD-2::GFP (top) and MKS-2::mSc (middle) in cilia of control and *inpp-1* mutant (two representative cilia; a,b) animals. Cilium proper oriented to the left; scale, 2 μm. (I) Mean fluorescence intensity and (J) volume of PKD-2::GFP in the cilium proper of control and *inpp-1* mutants, n ≥ 44. Data are represented as mean +/- SEM; Mann-Whitney test, * $p < 0.05$.

Figure 4. An increase in ciliary $PI(4,5)P_2$ does not impact the length of the cilium proper. (A) Representative images of RnB cilia filled out with KLP-6::GFP (top) in

control, PPK-1 Oex, and *inpp-1* mutant animals. Distal tip is to the right; MKS-2::mSc (middle) marks the TZ; scale, 2 µm. (B) Ciliary length was unchanged in the PPK-1 Oex and *inpp-1* mutant compared to the control; n ≥ 45. Data are represented as mean +/- SEM, mixed-effects model (REML). (C) Model; PPK-1 and INPP-1 regulate $PI(4,5)P_2$ abundance and localization in the RnB ciliated sensory neurons. $PI(4,5)P_2$ is normally absent from the cilium proper (left). Overexpression of PPK-1 (middle) increases $PI(4,5)P_2$ in the PCMC, which leads to a decrease in CLHM-1 abundance and EV shedding. Loss of *inpp-1* (right) results in accumulation of $PI(4,5)P_2$ in the cilium proper and an increase in PKD-2 EV shedding. Manipulation of $PI(4,5)P_2$ levels did not impact cilium length.

Materials and Methods

C. elegans strains and maintenance

All strains were cultured at 20°C on Nematode Growth Media (NGM) plates seeded with OP50 *E. coli*. *inpp-1(gk3262)* IV and *him-5(e1490)* V mutant alleles, *ppk-1*(*syb8819 [mNG::ppk-1])* I, *mks-2*(*oq101 [mks-2::mNG]*) II, *mks-2(syb7299 [mks-2::mSc])* II, and *inpp-1(syb3371 [inpp-1::mNG]) IV* endogenous insertion alleles, *gqIs25 [rab-3 promoter::ppk-1]* I, *myIs10 [klp-6 promoter::klp-6::GFP]*, and *henIs1 [klp-6 promoter::mNG::PLCδ1-PH]* V integrated transgenes, and *henSi3 [clhm-1 promoter::clhm-1::tdT]* III, *henSi20 [pkd-2 promoter::pkd-2::GFP]* IV, and *henSi21 [pkd-2 promoter::pkd-2::GFP]* V single copy transgenes were used. See SI Appendix, Table S1 for a list of all strains used in this work.

Generation of the PI(4,5)P_2 sensor

The construct used to express the PI(4,5)P_2 sensor mNG::PLCδ1-PH in the EVNs was created using restriction enzymes for cloning. mNG containing synthetic introns, with no stop codon, and followed by the flexible linker GSSGSSGTS was amplified from Addgene plasmid #177338 pGLOW77 (46) and inserted into pENM1, a plasmid which contains the 1.58 kb *klp-6* promoter (23). The PH domain of phospholipase C delta 1 (47) was amplified from Addgene plasmid #21179 (GFP-C1-PLCdelta-PH) and inserted following the flexible linker at the C-terminal end of mNG. This *klp-6* promoter:: mNG::PLCδ1-PH plasmid pJT174 (2 ng/µl), pCFJ421 (*myo-2* promoter::GFP::H2B; 5 ng/µl) (48), and genomic DNA (90 ng/µl) were injected into wild-type animals using the standard germline transformation technique (49). Part of the resulting extrachromosomal array was integrated into the *him-5* locus using CRISPR/Cas9 genome editing. Two gRNAs specific for the *him-5* locus and one gRNA to target the pJT174 backbone to fragment the extrachromosomal array were injected along with a *dpy-10* cRNA and *dpy-10* repair oligonucleotide harboring the dominant *cn64* mutation. In the F1 generation, we cloned animals with the dominant Roller phenotype to enrich for animals with CRISPR/Cas9 edits (50). We screened resulting F2 progeny and selected four plates that appeared to have significantly more animals with GFP in the nuclei of the pharyngeal muscles (pCFJ421) compared to the starting strain with extrachromosomal array. Eight worms were cloned from each of these plates and the F3 animals were screened for fluorescence. One plate had animals that exhibited 100% fluorescence and a *him* phenotype; this integrated transgene is designated *henIs1.*

Cilia imaging and analysis

Imaging of RnB neurons was performed on adult males 24 hours post fourth larval (L4) stage. *C. elegans* were immobilized with 50mM levamisole (ThermoFisher Cat #: AC187870100) pipetted onto 3% agarose pads on microscope slides and Z-stack images of splayed male tails were acquired with an Andor Dragonfly microscope (63x objective) and Zyla sCMOS camera. Identical image acquisition settings were used for all images that were directly compared; control and experimental strains were always imaged on the same day. The “multi plot” function in ImageJ (NIH) was used to plot fluorescence intensity distribution of mNG::PLCδ1-PH, mNG::PPK-1, or INPP-1::mNG along a 6 µm linear ROI that was drawn through the entirety of the cilium and base for RnB2-RnB5 neurons. For each measurement, the center of the transition zone as determined by MKS-2::mSc fluorescence was positioned at 3 µm. In normalized intensity plots, all values were normalized to the maximum intensity value in the ROI.

Imaris (Oxford Instruments) was used for quantitative volumetric and fluorescence intensity analysis of the cilium proper and cilium base in three-dimensional reconstructions. A ROI was drawn around the ciliary region of each RnB analyzed and a constant, preset intensity threshold, which was dependent on the fluorescent protein being analyzed, was used to select the fluorescence signal and create a corresponding surface using the surfaces tool in the cilium proper and ciliary base (Sup. Fig. 2). For ciliary length analysis, surfaces were first made to encapsulate the transition zone. A ROI was then drawn to exclude the transition zone surface but enclose the KLP-6::GFP-labeled cilium proper. The filament tool was used to draw the cilium structure in 3D space given a set segment seed point threshold (=160); lengths of each filament were recorded.

EV imaging and analysis

Eight transgenic L4 hermaphrodites carrying the *him-5(e1490)* mutation and single copy transgenes expressing fluorescent protein-tagged EV cargos were picked to 6 cm NGM plates and allowed to grow for 4 days, resulting in a mixed population of adult males and hermaphrodites. Adult males were picked from an unseeded region of the NGM plate to prevent contamination from the *E. coli* food source, then picked into 20 mM levamisole (100 mM diluted in IMage-iT FX Signal Enhancer medium; ThermoFisher Item no. I36933) on 3% agarose pads on slides and covered with high-performance cover glass (Zeiss, Item no. 474030-9020-000). To prevent contaminating signal from dust and other particles, the high-performance cover glass was placed in a coverslip holder, cleaned with 200-proof ethanol for 30 minutes (ThermoFisher Item no. 04-355-451), rinsed three times with HPLC H2O shaking for 10 minutes (ThermoFisher Item no. W5-4), then covered with foil and dried on a heat block. EV images were collected with an Andor Dragonfly microscope and Andor Zyla sCMOS detector using total internal reflection fluorescence (TIRF) microscopy. The TIRF angle of incidence was manually adjusted for each animal to achieve critical angle. All images of released EVs were taken 30 ± 5 minutes after each animal was immobilized on the agar pad. Imaris software (Oxford Instruments) was used to quantitate the number of EVs released into the environment from each male tail. EVs were identified using the “Spot” function, setting object size to 0.350 μm in diameter. A quality threshold was set for each dataset, as determined by analysis of negative controls. Hot pixels were manually removed. EVs that contained both PKD-2 and CLHM-1 were

identified as GFP and RFP spots with a maximum distance of 0.3 µm; these data are presented as the probability of PKD-2::GFP being found in a CLHM-1::tdT EV.

Statistical Analysis

All statistical analyses and graphing were performed using GraphPad Prism version 10.1.2. Dataset normality was determined using the Anderson-Darling normality test. Depending on normality, either the Student's *t* test or Mann-Whitney U test was used when comparing two datasets and one-way ANOVA or Kruskal-Wallis test with multiple comparisons when comparing three or more datasets (*p< 0.05, **p< 0.01, ***p< 0.001). Statistical details for individual experiments are specified in the figure legends.

Data Availability

Original data have been deposited at Mendeley Data and will be publicly available as of the date of publication. Individual image files as well as any additional information required to reanalyze the data are available from the corresponding author upon request.

Acknowledgments

We thank the *Caenorhabditis* Genetics Center, which is supported by the NIH-ORIP (P40 OD010440) for strains. Microscopy access was supported by grants from the NIH-NIGMS P20 GM103446, the NIGMS P20 GM139760, and the State of Delaware; microscopy equipment was acquired with NIGMS S10 OD030321. This work was

supported by NIH-NIGMS T32 GM133395 (to M.E. as part of the Chemistry Biology Interface predoctoral training program), a University of Delaware Graduate Scholars award (to M.E.), NIH Common Fund R03 TR004480 (to J.E.T.) and NIH-NIGMS R01 GM135433 (to J.E.T.).

Author Contributions

Research Design, M.E., A.E.S., and J.E.T.; Methodology, M.E., A.E.S., and J.E.T.; Data Collection, M.E., A.E.S., N.S.P., and K.D.P.; Data Analysis, M.E., A.E.S., and N.S.P.; Writing – original draft, M.E., A.E.S., and J.E.T; Writing – review and editing, M.E., A.E.S., N.S.P., K.D.P., and J.E.T; Visualization, M.E.; Supervision, J.E.T.; Funding Acquisition, M.E., and J.E.T.

Declaration of Interests

The authors declare no competing interests

References

1. P. Mill, S. T. Christensen, L. B. Pedersen, Primary cilia as dynamic and diverse signalling hubs in development and disease. *Nat. Rev. Genet.* **24**, 421–441 (2023).

2. C. R. Wood, K. Huang, D. R. Diener, J. L. Rosenbaum, The Cilium Secretes Bioactive Ectosomes. *Curr. Biol.* **23**, 906–911 (2013).

3. R. Luxmi, D. Kumar, R. E. Mains, S. M. King, B. A. Eipper, Cilia-based peptidergic signaling. *PLoS Biol.* **17**, e3000566 (2019).

4. J. Wang, *et al.*, C. elegans Ciliated Sensory Neurons Release Extracellular Vesicles that Function in Animal Communication. *Curr. Biol.* **24**, 519–525 (2014).

5. J. Wang, I. A. Nikonorova, A. Gu, P. W. Sternberg, M. M. Barr, Release and targeting of polycystin-2-carrying ciliary extracellular vesicles. *Curr. Biol.* **30**, R755–R756 (2020).

6. A. R. Nager, *et al.*, An Actin Network Dispatches Ciliary GPCRs into Extracellular Vesicles to Modulate Signaling. *Cell* **168**, 252-263.e14 (2017).

7. R. Luxmi, S. M. King, Cilia-derived vesicles: An ancient route for intercellular communication. *Semin. Cell Dev. Biol.* **129**, 82–92 (2022).

8. M. Cao, *et al.*, Uni-directional ciliary membrane protein trafficking by a cytoplasmic retrograde IFT motor and ciliary ectosome shedding. *Elife* **4**, e05242 (2015).

9. I. Ojeda Naharros, M. V Nachury, Shedding of ciliary vesicles at a glance. *J. Cell Sci.* **135** (2022).

10. K. Park, M. R. Leroux, Composition, organization and mechanisms of the transition zone, a gate for the cilium. *EMBO Rep.* **23**, e55420 (2022).

11. V. L. Jensen, *et al.*, Formation of the transition zone by Mks5/Rpgrip1L establishes a ciliary zone of exclusion (CIZE) that compartmentalises ciliary signalling proteins and controls PIP2 ciliary abundance. *EMBO J.* **34**, 2537–2556

(2015).

12. T. Balla, Phosphoinositides: tiny lipids with giant impact on cell regulation. *Physiol. Rev.* **93**, 1019–1137 (2013).

13. S. E. Conduit, B. Vanhaesebroeck, Phosphoinositide lipids in primary cilia biology. *Biochem. J.* **477**, 3541–3565 (2020).

14. D. Weinkove, *et al.*, Overexpression of PPK-1, the Caenorhabditis elegans Type I PIP kinase, inhibits growth cone collapse in the developing nervous system and causes axonal degeneration in adults. *Dev. Biol.* **313**, 384–397 (2008).

15. J. C. Loijens, R. A. Anderson, Type I phosphatidylinositol-4-phosphate 5-kinases are distinct members of this novel lipid kinase family. *J. Biol. Chem.* **271**, 32937–32943 (1996).

16. F. R. Garcia-Gonzalo, *et al.*, Phosphoinositides Regulate Ciliary Protein Trafficking to Modulate Hedgehog Signaling. *Dev. Cell* **34**, 400–409 (2015).

17. M. Chávez, *et al.*, Modulation of Ciliary Phosphoinositide Content Regulates Trafficking and Sonic Hedgehog Signaling Output. *Dev. Cell* **34**, 338–350 (2015).

18. K. Ukhanov, *et al.*, INPP5E controls ciliary localization of phospholipids and the odor response in olfactory sensory neurons. *J. Cell Sci.* **135** (2022).

19. S. L. Bielas, *et al.*, Mutations in INPP5E, encoding inositol polyphosphate-5-phosphatase E, link phosphatidyl inositol signaling to the ciliopathies. *Nat. Genet.* **41**, 1032–1036 (2009).

20. M. Jacoby, *et al.*, INPP5E mutations cause primary cilium signaling defects, ciliary

566 instability and ciliopathies in human and mouse. *Nat. Genet.* **41**, 1027–1031
567 (2009).

568 21. S. C. Phua, *et al.*, Dynamic Remodeling of Membrane Composition Drives Cell
569 Cycle through Primary Cilia Excision. *Cell* **168**, 264-279.e15 (2017).

570 22. J. Wang, *et al.*, Sensory cilia act as a specialized venue for regulated extracellular
571 vesicle biogenesis and signaling. *Curr. Biol.* **31**, 3943-3951.e3 (2021).

572 23. M. Clupper, *et al.*, Kinesin-2 motors differentially impact biogenesis of
573 extracellular vesicle subpopulations shed from sensory cilia. *iScience* **25**, 105262
574 (2022).

575 24. G. van Niel, G. D'Angelo, G. Raposo, Shedding light on the cell biology of
576 extracellular vesicles. *Nat. Rev. Mol. Cell Biol.* **19**, 213–228 (2018).

577 25. J. Wang, *et al.*, Cell-Specific Transcriptional Profiling of Ciliated Sensory Neurons
578 Reveals Regulators of Behavior and Extracellular Vesicle Biogenesis. *Curr. Biol.*
579 **25**, 3232–3238 (2015).

580 26. A. Razzauti, P. Laurent, Ectocytosis prevents accumulation of ciliary cargo in C.
581 elegans sensory neurons. *Elife* **10**, e67670 (2021).

582 27. J. Wang, *et al.*, Ciliary intrinsic mechanisms regulate dynamic ciliary extracellular
583 vesicle release from sensory neurons. *Curr. Biol.* **34**, 2756-2763.e2 (2024).

584 28. J. E. Maguire, *et al.*, Myristoylated CIL-7 regulates ciliary extracellular vesicle
585 biogenesis. *Mol. Biol. Cell* **26**, 2823–2832 (2015).

586 29. M. Katan, S. Cockcroft, Phosphatidylinositol(4,5)bisphosphate: diverse functions

at the plasma membrane. *Essays Biochem.* **64**, 513–531 (2020).

30. R. O'Hagan, *et al.*, Glutamylation Regulates Transport, Specializes Function, and Sculpts the Structure of Cilia. *Curr. Biol.* **27**, 3430-3441.e6 (2017).

31. M. Silva, *et al.*, Cell-Specific α-Tubulin Isotype Regulates Ciliary Microtubule Ultrastructure, Intraflagellar Transport, and Extracellular Vesicle Biology. *Curr. Biol.* **27**, 968–980 (2017).

32. E. M. Peden, M. M. Barr, The KLP-6 Kinesin Is Required for Male Mating Behaviors and Polycystin Localization in Caenorhabditis elegans. *Curr. Biol.* **15**, 394–404 (2005).

33. D. DiTirro, A. Philbrook, K. Rubino, P. Sengupta, The Caenorhabditis elegans Tubby homolog dynamically modulates olfactory cilia membrane morphogenesis and phospholipid composition. *Elife* **8**, e48789 (2019).

34. K. I. Lange, S. Tsiropoulou, K. Kucharska, O. E. Blacque, Interpreting the pathogenicity of Joubert syndrome missense variants in Caenorhabditis elegans. *Dis. Model. Mech.* **14**, dmm046631 (2021).

35. A. Molla-Herman, *et al.*, The ciliary pocket: an endocytic membrane domain at the base of primary and motile cilia. *J. Cell Sci.* **123**, 1785–1795 (2010).

36. J. Hodgkin, H. R. Horvitz, S. Brenner, Nondisjunction Mutants of the Nematode CAENORHABDITIS ELEGANS. *Genetics* **91**, 67 (1979).

37. S. Stilling, T. Kalliakoudas, H. Benninghoven-Frey, T. Inoue, B. H. Falkenburger, PIP(2) determines length and stability of primary cilia by balancing membrane

608 turnovers. *Commun. Biol.* **5**, 93 (2022).

609 38. S. Mukhopadhyay, *et al.*, The ciliary G-protein-coupled receptor Gpr161
610 negatively regulates the Sonic hedgehog pathway via cAMP signaling. *Cell* **152**,
611 210–223 (2013).

612 39. S. Mukhopadhyay, *et al.*, TULP3 bridges the IFT-A complex and membrane
613 phosphoinositides to promote trafficking of G protein-coupled receptors into
614 primary cilia. *Genes Dev.* **24**, 2180–2193 (2010).

615 40. J. Srinivasan, *et al.*, A blend of small molecules regulates both mating and
616 development in Caenorhabditis elegans. *Nature* **454**, 1115–1118 (2008).

617 41. X. Zhang, A. B. Jefferson, V. Auethavekiat, P. W. Majerus, The protein deficient in
618 Lowe syndrome is a phosphatidylinositol-4,5-bisphosphate 5-phosphatase. *Proc.*
619 *Natl. Acad. Sci. U. S. A.* **92**, 4853–4856 (1995).

620 42. S. E. Conduit, J. M. Dyson, C. A. Mitchell, Inositol polyphosphate 5-
621 phosphatases; new players in the regulation of cilia and ciliopathies. *FEBS Lett.*
622 **586**, 2846–2857 (2012).

623 43. Y. Rbaibi, *et al.*, OCRL1 modulates cilia length in renal epithelial cells. *Traffic* **13**,
624 1295–1305 (2012).

625 44. N. Luo, *et al.*, OCRL localizes to the primary cilium: a new role for cilia in Lowe
626 syndrome. *Hum. Mol. Genet.* **21**, 3333–3344 (2012).

627 45. N. Luo, *et al.*, Compensatory Role of Inositol 5-Phosphatase INPP5B to OCRL in
628 Primary Cilia Formation in Oculocerebrorenal Syndrome of Lowe. *PLoS One* **8**,

e66727 (2013).

46. G. Witten, *et al.*, mScarlet and split fluorophore mScarlet resources for plasmid-based CRISPR/Cas9 knock-in in C. elegans. *microPublication Biol.* (2023).

47. T. P. Stauffer, S. Ahn, T. Meyer, Receptor-induced transient reduction in plasma membrane PtdIns(4,5)P2 concentration monitored in living cells. *Curr. Biol.* **8**, 343–346 (1998).

48. C. Frøkjær-Jensen, M. W. Davis, M. Ailion, E. M. Jorgensen, Improved Mos1-mediated transgenesis in C. elegans. *Nat. Methods* **9**, 117-8 (2012).

49. C. C. Mello, J. M. Kramer, D. Stinchcomb, V. Ambros, Efficient gene transfer in C.elegans: Extrachromosomal maintenance and integration of transforming sequences. *EMBO J.* **10**, 3959–3970 (1991).

50. J. A. Arribere, *et al.*, Efficient marker-free recovery of custom genetic modifications with CRISPR/Cas9 in Caenorhabditis elegans. *Genetics* **198**, 837–846 (2014).

Figure 1

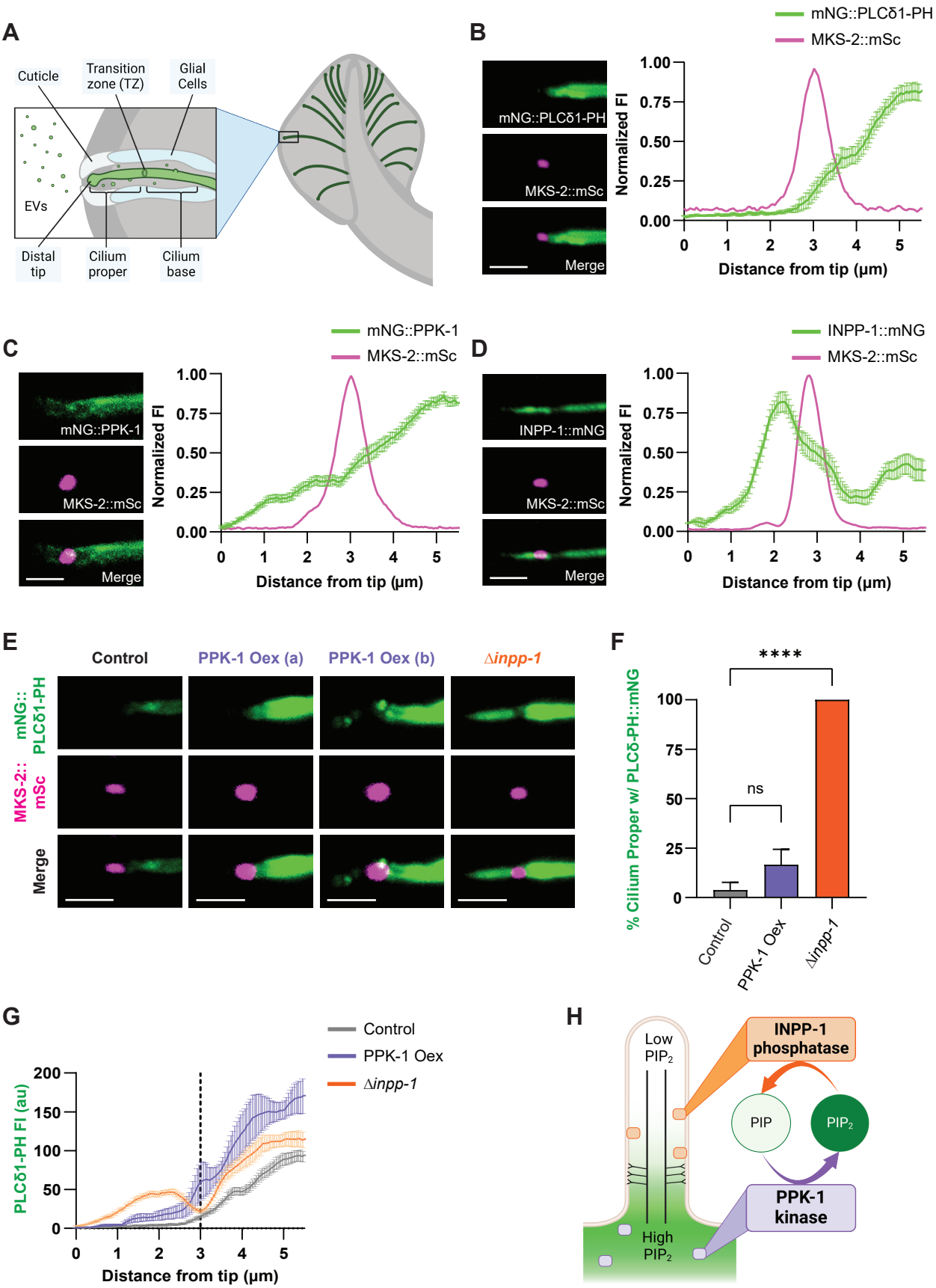

Figure 2

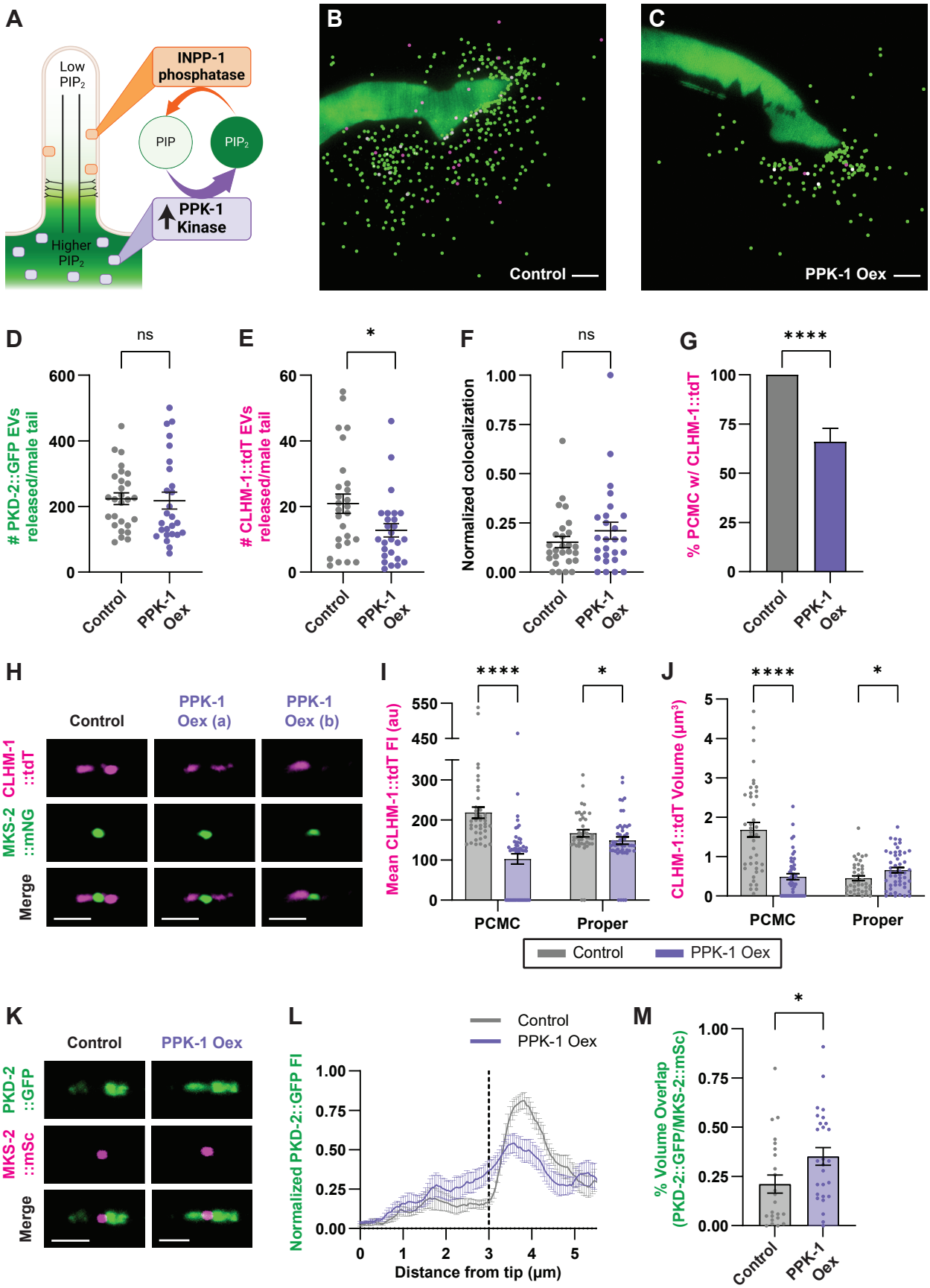

Figure 3

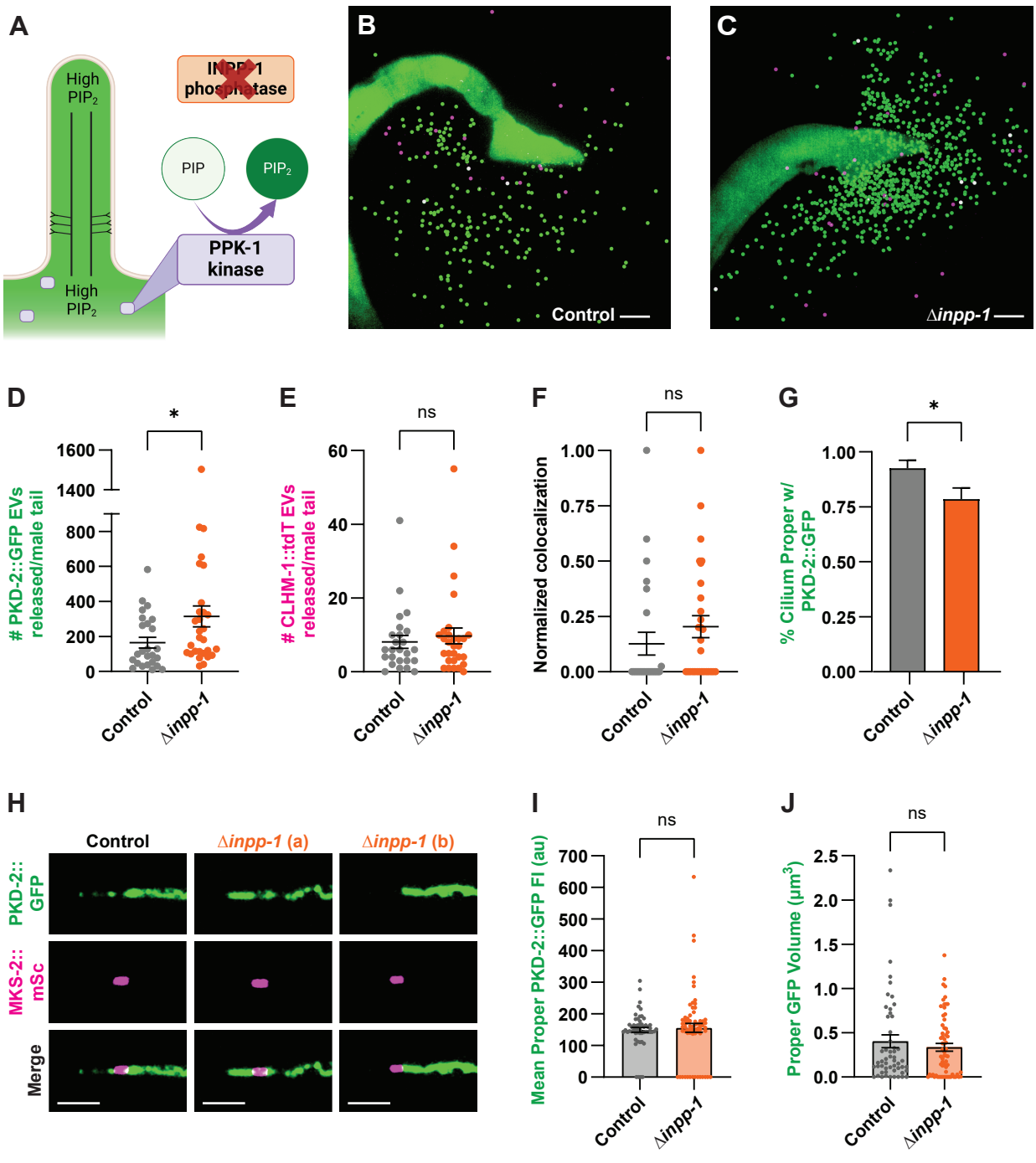

Figure 4